JKMS

Original Article
Basic Medical Sciences

Check for updates

Dawn of the Visible Monkey: Segmentation of the Rhesus Monkey for 2D and 3D Applications

Chung Yoh Kim [ID],[1] **Ae-Kyoung Lee** [ID],[2] **Hyung-Do Choi** [ID],[2] and **Jin Seo Park** [ID][1]

[1]Department of Anatomy, Dongguk University School of Medicine, Gyeongju, Korea
[2]Electronics and Telecommunications Research Institute, Daejeon, Korea

OPEN ACCESS

▶ See the editorial "A Series of Articles Based on a Long-Term Plan" in volume 35, number 15, e126.

ORCID iDs
Chung Yoh Kim [ID]
https://orcid.org/0000-0001-8074-076X
Ae-Kyoung Lee [ID]
https://orcid.org/0000-0002-8082-4194
Hyung-Do Choi [ID]
https://orcid.org/0000-0003-2652-7524
Jin Seo Park [ID]
https://orcid.org/0000-0001-7956-4148

Disclosure
The authors have no potential conflicts of interest to disclose.

ABSTRACT

Background: To properly utilize the sectioned images in a Visible Monkey dataset, it is essential to segment the images into distinct structures. This segmentation allows the sectioned images to be compiled into two-dimensional or three-dimensional software packages to facilitate anatomy and radiology education, and allows them to be used in experiments involving electromagnetic radiation. The purpose of the present study was to demonstrate the potential of the sectioned images using the segmented images.
Methods: Using sectioned images of a monkey's entire body, 167 structures were segmented using Adobe Photoshop. The segmented images and sectioned images were packaged into the browsing software. Surface models were made from the segmented images using Mimics. Volume models were made from the sectioned images and segmented images using MRIcroGL.
Results: In total, 839 segmented images of 167 structures in the entire body of a monkey were produced at 0.5-mm intervals (pixel size, 0.024 mm; resolution, 8,688 × 5,792; color depth, 24-bit color; BMP format). Using the browsing software, the sectioned images and segmented images were able to be observed continuously and magnified along with the names of the structures. The surface models of PDF file were able to be handled freely using Adobe Reader. In the surface models, the space information of all segmented structures was able to be identified using Sim4Life. On MRIcroGL, the volume model was able to be browsed and sectioned at any angle with real color.
Conclusion: Browsing software, surface models, and volume models are able to be produced based on the segmentation of the sectioned images. These will be helpful for students and researchers studying monkey anatomy and radiology, as well as for biophysicists examining the effects of electromagnetic radiation.

Keywords: Haplorhini; Visible Human Projects; Software; Three-Dimensional Imaging

INTRODUCTION

From veterinary medicine and evolutionary biology to biophysics, monkeys are useful animal models because of their similarities to humans.[1-3] Monkey researchers and students require a basic understanding of veterinary anatomy and radiology. While it is typically necessary to dissect a monkey for veterinary anatomy research, it is very difficult to obtain monkeys for

Author Contributions

Conceptualization: Park JS, Kim CY; Data curation: Lee AK, Choi HD, Park JS; Formal analysis: Kim CY; Methodology: Kim CY; Validation: Lee AK, Choi HD, Park JS; Investigation: Kim CY; Writing - original draft: Kim CY, Park JS.

dissection. Knowledge of sectional anatomy is required to interpret computed tomographs (CTs) and magnetic resonance images (MRIs) of monkeys,[4-7] but there is no sectional anatomy atlas of monkey which can show vividly normal structures on sectional planes in detail.

To overcome the difficulties of dissection and the lack of appropriate atlases of a monkey, computer software to deal with two-dimensional (2D) and three-dimensional (3D) images of monkey is need. Typically, 2D and 3D software packages rely upon CTs and MRIs. However, in the software based on the CTs and MRIs, anatomical structures cannot be shown in detail, because of the 8-bit gray scale and low resolution (pixel size and intervals, > 0.1 mm) of the raw data. Therefore, it is ideal for the 2D and 3D software packages to use high-resolution sectioned images in real color.[8-12]

We previously produced the sectioned images of a rhesus monkey (color depth, 48-bit color; intervals, > 0.05 mm; pixel size, 0.024 mm) in the Visible Monkey project.[13] Segmentation of the sectioned images is necessary to allow anatomical structures to be distinguished in the 2D and 3D software packages.[14-16]

The purpose of this study is to present the utility of the segmented images, made from the sectioned images of Visible Monkey, with regard to the learning of monkey anatomy and radiology. To achieve this objective, sectioned images of a rhesus monkey were segmented; these segmented images were used to create 2D software (browsing software) and 3D software (PDF file).

METHODS

In our previous study, sectioned images of an entire monkey body were created (intervals of head, 0.05 mm; intervals of the rest regions, 0.5 mm; pixel size, 0.024 mm; resolution, 8,688 × 5,792; color depth, 48-bit color; BMP format) (**Fig. 1A**).[13] One hundred sixty-seven structures to segment were selected (**Table 1**). Most structures were selected for the purposes of anatomy education. The cerebrum, cerebrospinal fluid, and eye structures were also selected for biophysical experiments.[17] For segmentation, sectioned images were chosen at 0.5-mm intervals.

Segmentation was performed using Photoshop CC 2015 (Adobe Systems, Inc., San Jose, CA, USA). The boundaries of structures in the sectioned images were chosen semi-automatically
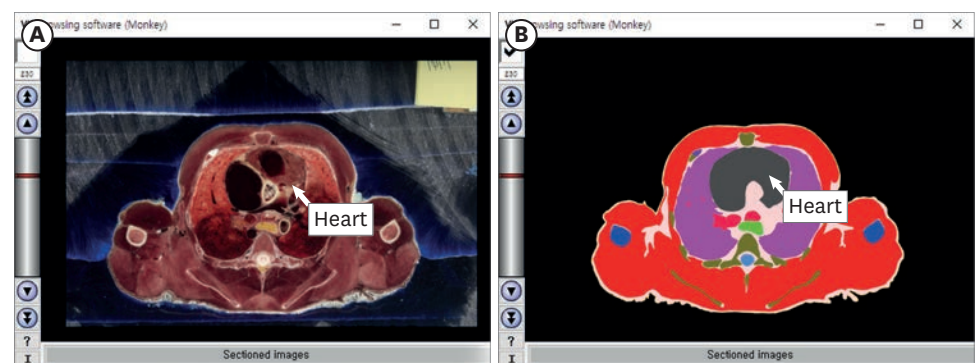
Fig. 1. Browsing software for a rhesus monkey. In the software, (**A**) the sectioned images and (**B**) segmented images of the thorax are able to be browsed serially. The name of the structure appears when a mouse pointer is placed over the image.

Table 1. One-hundred sixty-seven structures used for segmentation and surface modeling

Systems	Structures
Skeletal	Cranium, mandible, 1st to 7th cervical vertebrae, 1st to 12th thoracic vertebrae, 1st to 7th lumbar vertebrae, sacrum, caudal vertebrae, 1st to 12th ribs, costal cartilage, sternum, scapula, clavicle, humerus, radius, ulna, scaphoid, sesamoid bone, lunate, triquetrum, pisiform, trapezium, trapezoid, capitate, hamate, 1st to 5th metacarpal bones, phalanges of hand (1st to 5th proximal phalanges, 2nd to 5th middle phalanges, 1st to 5th distal phalanges), bones of pelvic girdle, femur, patella tibia, fibula, talus, calcaneus, navicular, medial cuneiform, intermediate cuneiform, lateral cuneiform, cuboid, 1st to 5th metatarsal bones, phalanges of foot (1st to 5th proximal phalanges, 2nd to 5th middle phalanges, 1st to 5th distal phalanges)
Articular	Intervertebral disc
Muscular	Muscle
Alimentary	Teeth, tongue, esophagus, stomach, small intestine, duodenum, large intestine, liver, gallbladder, common bile duct
Respiratory	Trachea, bronchi, lungs
Urinary	Kidney, urinary bladder, urethra
Genital	Ovary, uterus, vagina
Endocrine	Thyroid gland, adrenal gland
Cardiovascular	Heart, common carotid artery, external carotid artery, facial artery, superficial temporal artery, alveolar artery, internal carotid artery, middle cerebral artery, basilar artery, vertebral artery, internal jugular vein, retromandibular vein, superficial temporal vein, external jugular vein, anterior jugular vein, transverse sinus, confluence of sinuses, sigmoid sinus, superior sagittal sinus, straight sinus, the rest arteries, the rest veins
Lymphoid	Spleen
Central nervous	Spinal cord, brainstem, cerebrum (gray matter), cerebrum (white matter), dura mater, cerebrospinal fluid, cerebellum
Sensory	Sclera, cornea, lens (cortex), lens (nucleus), vitreous humor
Integumentary	Skin

using the quick selection tool and magnetic lasso tool, or manually using the lasso tool.[14] The boundaries were each filled automatically with a specific color using action and batch tools, then saved in BMP format to produce segmented images of an entire monkey body (**Fig. 1B**). To easily browse the sectioned images and segmented images, these images were converted from BMP format to JPG format and packaged into the browsing software (**Fig. 1**) created in our previous study.[10]

Surface modeling was performed using Mimics version 17.01 (Materialise, Leuven, Belgium). Each structure of the segmented images was remained using the threshold tool and reconstructed by surface modeling and saved in STL format. On Deep Exploration Standard (SAP America, Inc., Newtown Square, PA, USA), the STL files were assembled into a PDF file,[18] which allowed users to manipulate the surface models freely using Adobe Reader version 9 or higher (Adobe Systems, Inc.) (**Fig. 2**).

Volume modeling was carried out in MRIcroGL v1.0 (http://www.mccauslandcenter.sc.edu/mricrogl/) after converting sectioned images from BMP format to DICOM format using Photoshop. The DICOM files were imported and reconstructed automatically by volume modeling using the dcm2nii tool in MRIcroGL on a personal computer, thereby producing the volume model of the monkey body (**Fig. 3A and B**). In addition, based on the heart boundaries of segmented images, the heart alone was extracted from the images and saved in DICOM format using Photoshop. After the heart DICOM files had been reconstructed, a volume model of the heart was made using MRIcroGL (**Fig. 3C**).[19]

Spatial information of each segmented structure was checked by importing the STL files into Sim4Life (Zurich MedTech AG, Zurich, Switzerland) using a personal computer (operating system: Windows 10; Microsoft Corp., Redmond, WA, USA) (**Fig. 4**). Spatial volumes of segmented structures were multiplied by densities based on the Gabrial list and IT'IS foundation.[20,21] This enabled quantification of the weights of segmented structures.
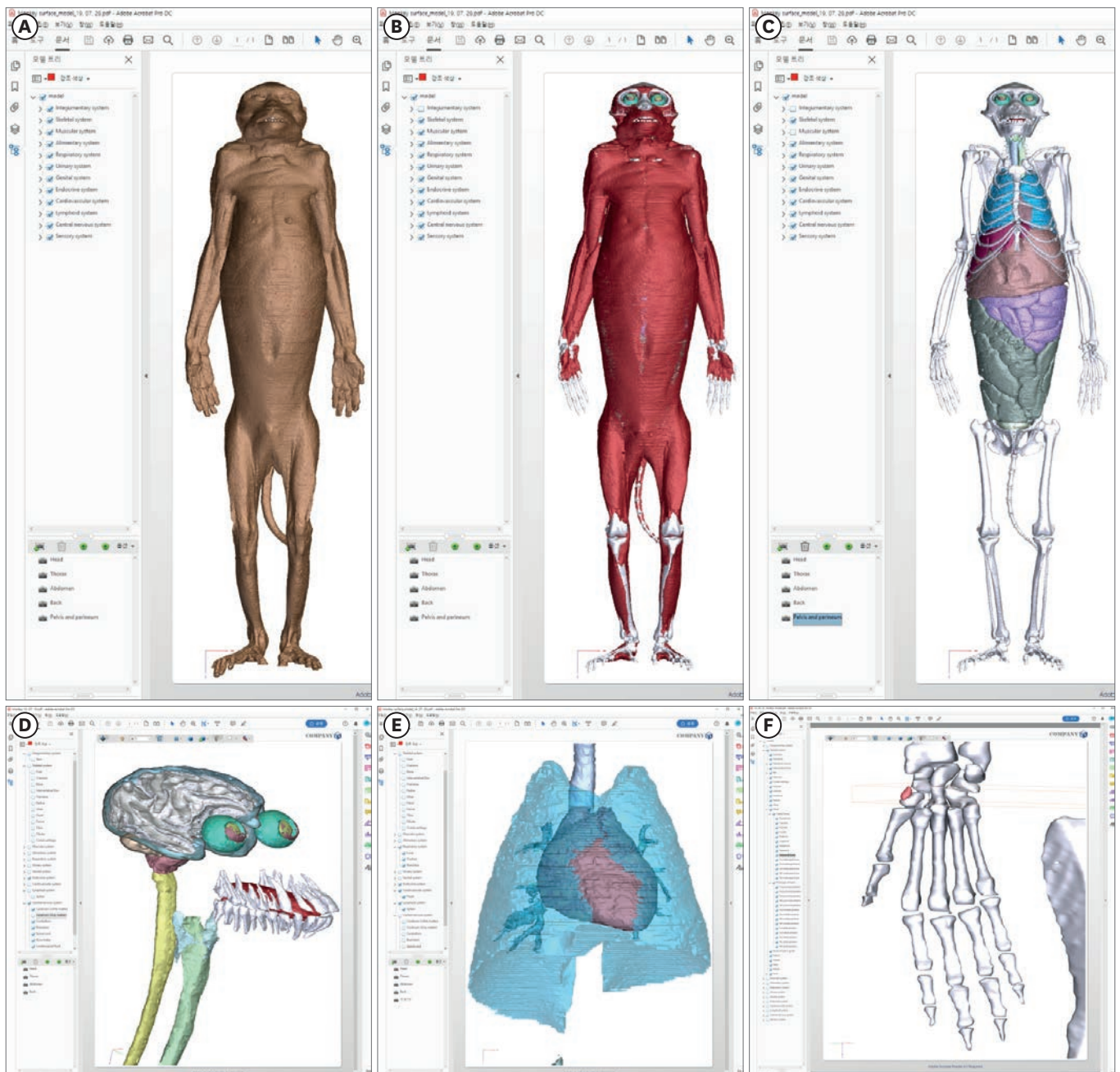
Fig. 2. Surface models of a rhesus monkey in Adobe Reader. The surface models of (**A**) the skin, (**B**) muscle, and (**C**) bones and organs are able to be displayed. (**D, E, F**) After the surface models are expanded, detailed shapes of segmented structures can be observed. (**F**) In front of the scaphoid, a sesamoid bone (red color) is visible.

RESULTS

This study produced 839 segmented images of 167 structures throughout a monkey (intervals, 0.5 mm; pixel size, 0.024 mm; resolution, 8,688 × 5,792; color depth, 24-bit color; BMP format; individual image size, 157 MB; total image size, 128 GB) (**Fig. 1**). Sectioned and segmented images could be observed continuously and magnified using the browsing software. The names of structures could be visualized using a mouse pointer (**Fig. 1**). The

Fig. 3. Volume models of a rhesus monkey on MRIcroGL. The volume models of (**A**) the whole body, (**B**) head, and (**C**) heart can be dissected at any angle (from left to right), similar to the dissection of a real cadaver.

surface models of 167 structures could be displayed and handled freely in a PDF file using Adobe Reader (file size, 52 MB) (**Fig. 2**). Using MRIcroGL, the real-color volume model of the whole body could be browsed and sectioned at any angle, similar to dissection of a real cadaver. Any region could be displayed in detail by magnification of the model (**Fig. 3B**). In addition, a volume model of the heart alone was able to be virtually dissected using MRIcroGL (**Fig. 3C**).

Some structures in monkey that definitely differ from structures in human were found using the browsing software, surface models, and volume models (**Fig. 5**). In the head, the eyeball, optic nerve, lateral geniculate nucleus, and hippocampus were relatively large (**Fig. 5A and C**)
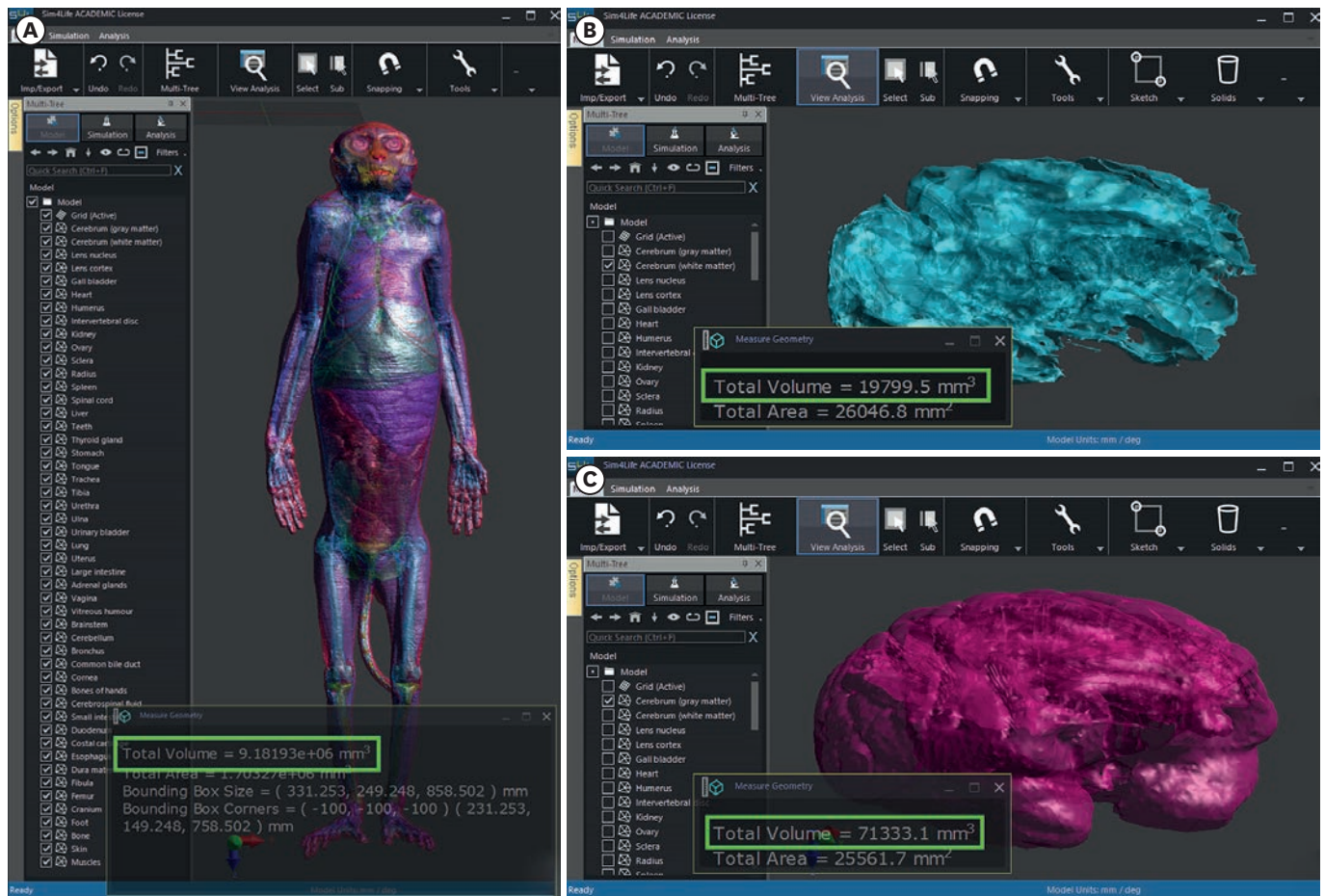
Fig. 4. Voxel models from STL files on Sim4Life software. (**A**) Voxel volumes (green box) of 167 structures in a whole monkey body, (**B**) white matter of the cerebrum, and (**C**) gray matter of the cerebrum are able to be measured.

because of the specialized primate visual system.[22] The salivary glands were also relatively large (**Fig. 3B**); large salivary glands are essential for wild animals because they must process tough food and digest raw food. In the wrist, the sesamoid bone was located in front of the scaphoid (**Fig. 2F**). In the thorax and abdomen, the anterior-posterior length of the torso was longer than its width (**Fig. 1**); wild animals, such as monkeys, have long torsos to facilitate quadrupedal movement.

The total spatial volume of the segmented structures was 9,181,930 mm^3. The volumes of gray matter (density, 1,039 kg/m^3) and white matter (density, 1,043 kg/m^3) in the cerebrum were 71,333.1 mm^3 and 19,799.5 mm^3, respectively; the weights of gray and white matter in the cerebrum were 74.11 g and 20.65 g, respectively (**Fig. 4**). The volume of the gray matter in the monkey was approximately 3.5-fold greater than volume of white matter, whereas the volume of gray matter in humans is two-fold greater than that of white matter. This is because monkeys require fewer and less varied connections (white matter) between gray matter, compared with humans.[23,24] The spatial volumes of all 167 structures could also be calculated.
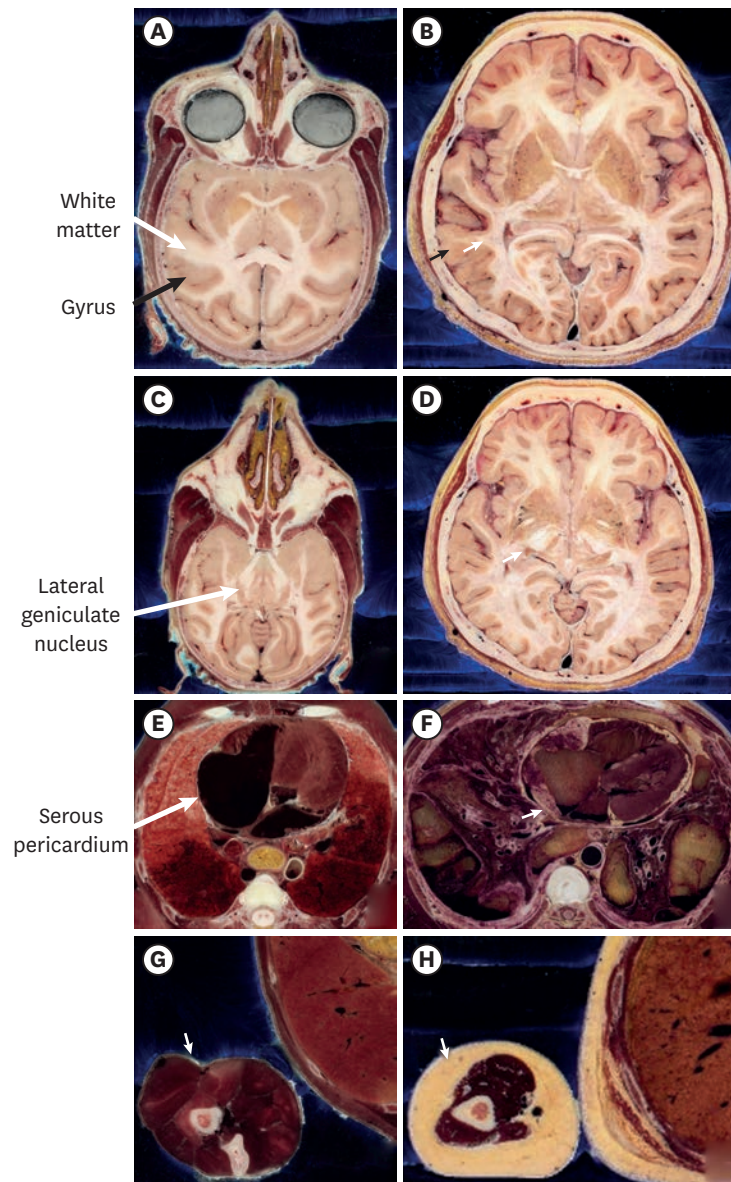
Fig. 5. Comparison of structures between a monkey and a human. In the head, (**A**) cerebral gyri of the monkey are simpler than (**B**) those of the human (black arrow). (**A**) The gray and white matter of the monkey are also simpler than (**B**) those of the human (white arrow). (**A**) The eyeball, optic nerve, (**C**) lateral geniculate nucleus (arrow), and hippocampus of the monkey are larger than (**D**) that of the human. (**E**) Because there is minimal fat in the monkey body, the rim of the heart and visceral layer of serous pericardium (arrow) of monkey are very clear, compared with (**F**) those of the human. (**G**) In the monkey, there is little fat (arrow) between skin and muscle, as well as between organs; (**H**) the human exhibits greater volumes of fat in both areas.

DISCUSSION

In the current study, segmented images were prepared from the sectioned images; 2D and 3D software packages were produced using both the sectioned and segmented images (**Figs. 1**-**3**). We established the utility of the segmented images of Visible Monkey as follows.

First, the segmented images were used to interpret the sectioned images. Structures on the sectioned images could not be interpreted without labels or the segmented images.

In this study, we assigned structure names (**Table 1**) to the sectioned images based on the segmented images in the browsing software.[14] A student could easily recognize the structure names using the browsing software (**Fig. 1**).

Second, the segmented images were used to reconstruct the surface models.[14] The surface models could not be reconstructed without the boundaries of each structure, which comprised the framework of the surface models. In this study, we created segmented images (**Fig. 1B**), then produced the surface models after stacking the boundaries (**Fig. 3**).

Furthermore, the surface models can be used for analysis of the effects of electromagnetic radiation on the body in biophysics research. Surface models contain spatial information of each structure in STL format. If tissue properties (e.g., density or weight) are transfused with spatial information such as this study (**Fig. 4**), the energy absorption of the tissues (i.e., specific absorption rate) can be virtually calculated from electromagnetic radiation.[24-27] In case of a monkey, in vivo experiment of the energy absorption can be performed. Finally, the result of virtual models of this study can be compared with the result of in vivo models to verify accuracy about effect of electromagnetic radiation by virtual models. If the accuracy of virtual models of monkey are proven, many virtual models of human in the world will be more positively used.

Third, the segmented images were used to reconstruct the volume models. Volume models of a single structure or small region are needed for medical training such as virtual ultrasonography of heart[28] and virtual arthroscopy of knee.[29] In case of the volume model of the entire body (**Fig. 3A and B**), the original resolution cannot be realized because of the limited capacity of a personal computer. In this study, we reconstructed volume models of a structure or small region using its segmented images (**Fig. 3C**).

Compared with CTs and MRIs, the sectioned images enable segmentation of more structures because of the improved color and resolution, whereas automatic and semiautomatic segmentations on the sectioned images are difficult because of this additional graphic information.[13,30] Nevertheless, in this study, some structures in sectioned images could be easily segmented for the following reasons.

First, in the sectioned images, the monkey brain was able to be segmented more easily than the human brain because of the simple gyri of the cerebrum. The number and curvature of monkey gyri are smaller and simpler, respectively (**Fig. 5A and C**), than those of the human gyri (**Fig. 5B and D**). Similarly, the curves of white matter in the monkey gyri are also simpler (**Fig. 5A and C**) than those of the human white matter (**Fig. 5B and D**). Consequently, we could semi-automatically segment the cerebral gyri of the monkey and automatically segment cerebral gray and white matter using Photoshop (**Fig. 4B and C**).

Second, segmentation of the monkey skin and muscle is easier than segmentation of the human skin and muscles because monkeys have minimal fat. Wild animals tend to be lean because they move frequently to survive. Although the monkey in the present study was reared in a laboratory, it had minimal fat in the skin and muscle. Also, the monkey had minimal fat around the visceral layer of serous pericardium (**Fig. 5E and G**), compared with the human (**Fig. 5F and H**). Therefore, we could easily segment the skin, muscle, and heart.

In 2019, the Visible Monkey project was launched based on sectioned images prepared from a monkey. The sectioned images first appeared on a computer; hence, the first study was

named the "Rise of the Visible Monkey,"[13] referring to the movie "Rise of the Planet of the Apes." In the present study, segmentation of the Visible Monkey was performed to produce 2D and 3D software packages. This highlighted the utility of the Visible Monkey; hence, the study was named "Dawn of the Visible Monkey," referring to the movie "Dawn of the Planet of the Apes."

In the near future, virtual reality and augmented reality systems[31] will be created based on 3D models with more detailed structures of the nervous system (e.g., nuclei and tracts of thalamus and hypothalamus, cranial nerves, spinal nerves with spinal ganglion, and blood vessels). To segment more detailed structures for virtual reality and augmented reality, anatomy experts must manually segment most structures, with some exceptions. This manual segmentation is difficult; therefore, the name of the future study may be "War for the Visible Monkey," referring to the movie "War for the Planet of the Apes."

In this study, to establish the utility of the sectioned images in Visible Monkey, 2D (browsing software) (**Fig. 1**) and 3D (surface models and volume models) (**Figs. 2** and **3**) software packages were produced. These software packages are expected to be useful for students of veterinary anatomy and radiology. Moreover, spatial information of the segmented structures can be analyzed based on the surface models, which may be useful for biophysical experiments.[24,25] Users will be able to download all data from this study after user certification by the Electronics and Telecommunications Research Institute.

REFERENCES

1. Thiebaut de Schotten M, Dell'Acqua F, Valabregue R, Catani M. Monkey to human comparative anatomy of the frontal lobe association tracts. *Cortex* 2012;48(1):82-96.
   PUBMED | **CROSSREF**

2. Olsen RG, Ballinger MB, David TD, Lotz WG. Rewarming of the hypothermic rhesus monkey with electromagnetic radiation. *Bioelectromagnetics* 1987;8(2):183-93.
   PUBMED | **CROSSREF**

3. Aversi-Ferreira TA, Aversi-Ferreira RA, Bretas RV, Nishimaru H, Nishijo H. Comparative anatomy of the arm muscles of the Japanese monkey (*Macaca fuscata*) with some comments on locomotor mechanics and behavior. *J Med Primatol* 2016;45(4):165-79.
   PUBMED | **CROSSREF**

4. Decramer T, Swinnen S, van Loon J, Janssen P, Theys T. White matter tract anatomy in the rhesus monkey: a fiber dissection study. *Brain Struct Funct* 2018;223(8):3681-8.
   PUBMED | **CROSSREF**

5. Besle J, Mougin O, Sánchez-Panchuelo RM, Lanting C, Gowland P, Bowtell R, et al. Is human auditory cortex organization compatible with the monkey model? Contrary evidence from ultra-high-field functional and structural MRI. *Cereb Cortex* 2019;29(1):410-28.
   PUBMED | **CROSSREF**

6. Schilling KG, Gao Y, Christian M, Janve V, Stepniewska I, Landman BA, et al. A web-based atlas combining MRI and histology of the squirrel monkey brain. *Neuroinformatics* 2019;17(1):131-45.
   PUBMED | **CROSSREF**

7. Gao Y, Chen W, Zhang X. Investigating the influence of spatial constraints on ultimate receive coil performance for monkey brain MRI at 7T. *IEEE Trans Med Imaging* 2018;37(7):1723-32.
   PUBMED | **CROSSREF**

8. Park JS, Shin HK, Shin BS, Kwon K. True-color face peeled images with botulinum toxin injection sites and anatomic landmarks. *Int J Morphol* 2019;37(3):1016-22.
   CROSSREF

9. Lee SB, Chung BS, Chung MS, Youn C, Park JS. Browsing software of the head sectioned images for the android mobile device. *Int J Morphol* 2017;35(4):1377-82.
   CROSSREF

10. Kwon K, Chung MS, Park JS, Shin BS, Chung BS. Improved software to browse the serial medical images for learning. *J Korean Med Sci* 2017;32(7):1195-201.
    PUBMED | CROSSREF

11. Kwon K, Shin HK, Shin BS, Park JS. Serially peeled images of the curved surface of the face based on cross-sectional images for use in plastic surgery. *J Plast Reconstr Aesthet Surg* 2016;69(5):727-9.
    PUBMED | CROSSREF

12. Park HS, Chung MS, Shin DS, Jung YW, Park JS. Whole courses of the oculomotor, trochlear, and abducens nerves, identified in sectioned images and surface models. *Anat Rec (Hoboken)* 2015;298(2):436-43.
    PUBMED | CROSSREF

13. Chung BS, Jeon CY, Huh JW, Jeong KJ, Har D, Kwack KS, et al. Rise of the Visible Monkey: sectioned images of rhesus monkey. *J Korean Med Sci* 2019;34(8):e66.
    PUBMED | CROSSREF

14. Park JS, Chung MS, Hwang SB, Lee YS, Har DH. Technical report on semiautomatic segmentation using the Adobe Photoshop. *J Digit Imaging* 2005;18(4):333-43.
    PUBMED | CROSSREF

15. Shin DS, Jang HG, Park JS, Park HS, Lee S, Chung MS. Accessible and informative sectioned images and surface models of a cadaver head. *J Craniofac Surg* 2012;23(4):1176-80.
    PUBMED | CROSSREF

16. Park JS, Chung MS, Chi JG, Park HS, Shin DS. Segmentation of cerebral gyri in the sectioned images by referring to volume model. *J Korean Med Sci* 2010;25(12):1710-5.
    PUBMED | CROSSREF

17. Yeom YS, Jeong JH, Kim CH, Han MC, Ham BK, Cho KW, et al. HDRK-Woman: whole-body voxel model based on high-resolution color slice images of Korean adult female cadaver. *Phys Med Biol* 2014;59(14):3969-84.
    PUBMED | CROSSREF

18. Park J, Chung B, Chung M. Digital anatomy using the surface models in portable document format file for self-learning and evaluation. *Digit Media* 2017;3(3):133-7.
    CROSSREF

19. Chung BS, Park JS. Real-color volume models made from real-color sectioned images of Visible Korean. *J Korean Med Sci* 2019;34(10):e86.
    PUBMED | CROSSREF

20. Gabriel C, Gabriel S, Corthout E. The dielectric properties of biological tissues: I. Literature survey. *Phys Med Biol* 1996;41(11):2231-49.
    PUBMED | CROSSREF

21. Christ A, Kainz W, Hahn EG, Honegger K, Zefferer M, Neufeld E, et al. The Virtual Family--development of surface-based anatomical models of two adults and two children for dosimetric simulations. *Phys Med Biol* 2010;55(2):N23-38.
    PUBMED | CROSSREF

22. Bragg EM, Fairless EA, Liu S, Briggs F. Morphology of visual sector thalamic reticular neurons in the macaque monkey suggests retinotopically specialized, parallel stream-mixed input to the lateral geniculate nucleus. *J Comp Neurol* 2017;525(5):1273-90.
    PUBMED | CROSSREF

23. Courchesne E, Chisum HJ, Townsend J, Cowles A, Covington J, Egaas B, et al. Normal brain development and aging: quantitative analysis at in vivo MR imaging in healthy volunteers. *Radiology* 2000;216(3):672-82.
    PUBMED | CROSSREF

24. Lee AK, Park JS, Hong SE, Taki M, Wake K, Wiart J, et al. Brain SAR of average male Korean child to adult models for mobile phone exposure assessment. *Phys Med Biol* 2019;64(4):045004.
    PUBMED | CROSSREF

25. Choi C, Nguyen TT, Yeom YS, Lee H, Han H, Shin B, et al. Mesh-type reference Korean phantoms (MRKPs) for adult male and female for use in radiation protection dosimetry. *Phys Med Biol* 2019;64(8):085020.
    PUBMED | CROSSREF

26. Neufeld E, Lloyd B, Schneider B, Kainz W, Kuster N. Functionalized anatomical models for computational life sciences. *Front Physiol* 2018;9:1594.
    PUBMED | CROSSREF

27. Park JS, Jung YW, Choi HD, Lee AK. VK-phantom male with 583 structures and female with 459 structures, based on the sectioned images of a male and a female, for computational dosimetry. *J Radiat Res (Tokyo)* 2018;59(3):338-80.
    PUBMED | CROSSREF

28. Werner H, Lopes J, Ribeiro G, Raposo AB, Trajano E, Araujo Júnior E. Three-dimensional virtual traveling navigation and three-dimensional printing models of a normal fetal heart using ultrasonography data. *Prenat Diagn* 2019;39(3):175-7.
   PUBMED | **CROSSREF**

29. Tofte JN, Westerlind BO, Martin KD, Guetschow BL, Uribe-Echevarria B, Rungprai C, et al. Knee, Shoulder, and Fundamentals of Arthroscopic Surgery Training: Validation of a Virtual Arthroscopy Simulator. *Arthroscopy* 2017;33(3):641-646.e3.
   PUBMED | **CROSSREF**

30. Chung BS, Han M, Har D, Park JS. Advanced sectioned images of a cadaver head with voxel size of 0.04 mm. *J Korean Med Sci* 2019;34(34):e218.
   PUBMED | **CROSSREF**

31. Andrews C, Southworth MK, Silva JN, Silva JR. Extended reality in medical practice. *Curr Treat Options Cardiovasc Med* 2019;21(4):18.
   PUBMED | **CROSSREF**